Northumbria Research Link

Citation: González-Avilés, J. J., Guzmán, F. S., Fedun, V., Verth, G., Sharma, R., Shelyag, Sergiy and Regnier, Stephane (2019) In situ generation of coronal Alfvén waves by jets. Monthly Notices of the Royal Astronomical Society, 484 (2). pp. 1936-1945. ISSN 0035-8711

Published by: Oxford University Press

URL: https://doi.org/10.1093/mnras/stz087 <https://doi.org/10.1093/mnras/stz087>

This version was downloaded from Northumbria Research Link: http://nrl.northumbria.ac.uk/id/eprint/38770/

Northumbria University has developed Northumbria Research Link (NRL) to enable users to access the University's research output. Copyright © and moral rights for items on NRL are retained by the individual author(s) and/or other copyright owners. Single copies of full items can be reproduced, displayed or performed, and given to third parties in any format or medium for personal research or study, educational, or not-for-profit purposes without prior permission or charge, provided the authors, title and full bibliographic details are given, as well as a hyperlink and/or URL to the original metadata page. The content must not be changed in any way. Full items must not be sold commercially in any format or medium without formal permission of the copyright holder. The full policy is available online: http://nrl.northumbria.ac.uk/policies.html

This document may differ from the final, published version of the research and has been made available online in accordance with publisher policies. To read and/or cite from the published version of the research, please visit the publisher's website (a subscription may be required.)

Northumbria University NEWCASTLE

University Library

Monthly Notices
of the
ROYAL ASTRONOMICAL SOCIETY

MNRAS **484,** 1936–1945 (2019)
Advance Access publication 2019 January 10

doi:10.1093/mnras/stz087

In situ generation of coronal Alfvén waves by jets

J. J. González-Avilés,[1★] F. S. Guzmán,[2★] V. Fedun,[3★] G. Verth,[4] R. Sharma,[5] S. Shelyag,[6] and S. Regnier[7]

[1]*Instituto de Geofísica, Unidad Michoacán, Universidad Nacional Autónoma de México, Antigua Carretera a Pátzcuaro 8701, 58190 Morelia, Michoacán, Mexico*
[2]*Laboratorio de Inteligencia Artificial y Supercómputo, Instituto de Física y Matemáticas, Universidad Michoacana de San Nicolás de Hidalgo. Edificio C3, Cd. Universitaria, 58040 Morelia, Michoacán, Mexico*
[3]*Department of Automatic Control and Systems Engineering, The University of Sheffield, Mappin Street, Sheffield S1 3JD, UK*
[4]*Solar Physics and Space Plasma Research Centre, School of Mathematics and Statistics, The University of Sheffield, Hicks Building, Hounsfield Road, Sheffield S3 7RH, UK*
[5]*Space Weather Research Group, Departmento de Física y Mathemáticas, Universidad de Alcalá (UAH), Calle el Escorial, 19-21, 28805 Alcalá de Henares, Spain*
[6]*School of Information Technology, Faculty of Science, Engineering and Built Environment, Deakin University, 221 Burwood Highway, Burwood, VIC 3125, Melbourne, Australia*
[7]*Department of Mathematics, Physics and Electrical Engineering, Northumbria University, Ellison Place, Newcastle upon Tyne NE1 8ET, UK*

Accepted 2019 January 6. Received 2019 January 4; in original form 2018 October 12

ABSTRACT

Within the framework of 3D resistive magnetohydrodynamic, we simulate the formation of a plasma jet with the morphology, upward velocity up to 130 km s^{-1}, and time-scale formation between 60 and 90 s after beginning of simulation, similar to those expected for type II spicules. Initial results of this simulation were published in paper by, e.g. González-Avilés et al. (2018), and present paper is devoted to the analysis of transverse displacements and rotational-type motion of the jet. Our results suggest that 3D magnetic reconnection may be responsible for the formation of the jet in paper by González-Avilés et al. (2018). In this paper, by calculating times series of the velocity components v_x and v_y in different points near to the jet for various heights we find transverse oscillations in agreement with spicule observations. We also obtain a time-distance plot of the temperature in a cross-cut at the plane $x = 0.1$ Mm and find significant transverse displacements of the jet. By analysing temperature isosurfaces of 10^4 K with the distribution of v_x, we find that if the line-of-sight (LOS) is approximately perpendicular to the jet axis then there is both motion towards and away from the observer across the width of the jet. This red–blue shift pattern of the jet is caused by rotational motion, initially clockwise and anti-clockwise afterwards, which could be interpreted as torsional motion and may generate torsional Alfvén waves in the corona region. From a nearly vertical perspective of the jet the LOS velocity component shows a central blue-shift region surrounded by red-shifted plasma.

Key words: MHD – methods: numerical – Sun: atmosphere.

1 INTRODUCTION

In the solar atmosphere, jet-like structures, defined as an impulsive evolution of collimated bright or dark structure are observed in a wide range of environments. In particular, the upper chromosphere is full with spicules, thin jets of chromospheric plasma that reach heights of 10,000 km or move above the photosphere. Although spicules were described by Secchi (1878), understanding their physical nature has been a whole area of research (Beckers et al. 1968; Sterling 2000). There are two types of spicules, the first type of spicules are so-called type I, which reach maximum heights of 4–8 Mm, maximum ascending velocities of 15–40 km s^{-1}, have a lifetime of 3–6.5 min (Pereira, De Pontieu & Carlsson 2012), and show up- and downward motions (Beckers et al. 1968; Suematsu, Wangm & Zirin 1995). These type I spicules are probably the counterpart of the dynamic fibrils. They follow a parabolic (ballistic) path in space and time. In general, the dynamics of these spicules are produced by mangnetoacoustic shock waves passing or wave-driving through the chromosphere (Shibata et al. 1982; De Pontieu, Erdélyi & James 2004; Hansteen et al. 2006; Martínez-Sykora, Hansteen & Carlsson 2009; Matsumoto & Shibata 2010; Scullion et al. 2011).The second type of spicules is called type II,

★ E-mail: jjgonzalez@igeofisica.unam.mx (JJG-A); guzman@ifm.umich.mx (FSG); v.fedun@sheffield.ac.uk (VF)

© 2019 The Author(s)
Published by Oxford University Press on behalf of the Royal Astronomical Society

Downloaded from https://academic.oup.com/mnras/article-abstract/484/2/1936/5287990 by University of Northumbria user on 04 April 2019

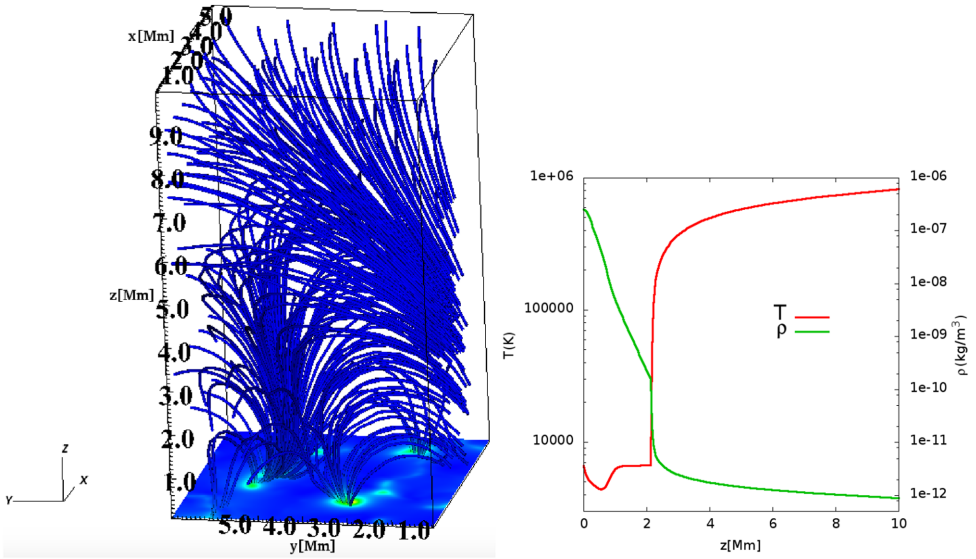

Figure 1. (Left) Magnetic field lines in the 3D domain at initial time. (Right) Temperature and mass density as a function of height z for the C7 equilibrium solar atmosphere model.

which reaches maximum heights of 3–9 Mm (longer in coronal holes) and have lifetimes of 50–150 s, shorter than that of type I spicules (De Pontieu, McIntosh & Hansteen 2007a; Pereira et al. 2012). These type II spicules show apparent upward motion with speeds of order 30–110 km s^{-1}. At the end of their life they usually exhibit rapid fading in chromospheric lines (De Pontieu et al. 2007b). It has been suggested from observations that type II spicules are continuously accelerated while being heated to at least transition region temperatures (De Pontieu et al. 2009, 2011). Other observations indicate that some type II spicules also show an increase or a more complex velocity dependence with height (Sekse, Rouppe van der Voort & De Pontieu 2012).

Also, type II spicules show other motions in addition to radial outflow. In the Ca II H line they are seen to sway transversely with amplitudes of order 10–20 km s^{-1} and periods of 100–500 s (De Pontieu et al. 2007b; Tomczyk et al. 2007; Zaqarashvili & Erdélyi 2009; McIntosh et al. 2011; Sharma, Verth & Erdélyi 2017), suggesting generation of upward, downward, and standing Alfvén waves (Okamoto & De Pontieu 2011; Tavabi, Koutchmy & Golub 2015), the generation of magnetohydrodynamic (MHD) kink mode waves or Alfvén waves due to magnetic reconnection (Nishizuka et al. 2008; He et al. 2009; Kuridze et al. 2012; McLaughlin et al. 2012) or due to magnetic tension and ambipolar diffusion (Martínez-Sykora et al. 2017). For instance, Suematsu et al. (2008) suggest that some spicules show multi-thread structure as a result of possible rotation. Another possible motion of type II spicules is the torsional one as suggested by Beckers (1972) and Kayshap et al. (2018), and established using high-resolution spectroscopy at the limb (De Pontieu et al. 2012). According to the latter, type II spicules show torsional motions with rotational speeds of 25–30 km s^{-1}. In addition, the continuation of this kind of motion in the transition region and coronal lines suggest that they may help driving the solar wind (McIntosh et al. 2011).

There are other types of motion less well established, for instance Curdt & Tian (2011) and Curdt, Tian & Kamio (2012) suggest that the spinning motion of type II spicules can explain the tilts of ultraviolet lines in the so-called explosive events producing larger-scale macro spicules. These spectral-line tilts were observed at the limb and also attributed to spicule rotation (Beckers 1972). At smaller scales, evidence of rotating motions has been deduced for the chromospheric/transition region jet events (Liu et al. 2009, 2011). In addition, Tian et al. (2014) using the Interface Region Imaging Spectrograph (IRIS) instrument found transverse motions as well as line broadening attributed to the existence of twist and torsional Alfvén waves. At the photospheric level, there is evidence that a fraction of spicules present twisting motions (Sterling, Harra & Moore 2010a; Sterling, Moore & DeForest 2010b; De Pontieu et al. 2012). Beyond the resolution of imaging instruments, the spectrum of explosive events can also be interpreted as arising from the fast rotation of magnetic structures (Curdt & Tian 2011; Curdt et al. 2012). Apart from the small scale jets, Doppler images have shown that several coronal jet events present strong rotational motion, diagnosed with blue–red shift observed on opposite sides of each jet (Dere, Bartoe & Brueckner 1989; Pike& Mason 1998; Cheung et al. 2015).

In this paper, we show that the jet with characteristics of a type II spicule, obtained in the numerical simulations presented in González-Avilés et al. (2018) shows transverse displacements and rotational-type motion initially clockwise and anti-clockwise afterwards, that could be a driver to excite torsional Alfvén waves directly in the corona.

The summary of the model and numerical methods are described in Section 2. Section 3 describes the analysis of the plasma motions in the jet. In Section 4, we present our final comments and conclusions.

2 SUMMARY OF THE MODEL AND NUMERICAL METHODS

The details of the numerical methods can be found in González-Avilés et al. (2018), and a brief summary is the following. We solve the resistive 3D MHD equations including the constant gravity field at the Sun's surface. We integrate the Extended Generalized Lagrange Multiplier (EGLM) resistive MHD (Jiang, Fang & Chen 2012) using High Resolution Shock Capturing methods with an

Downloaded from https://academic.oup.com/mnras/article-abstract/484/2/1936/5287990 by University of Northumbria user on 04 April 2019

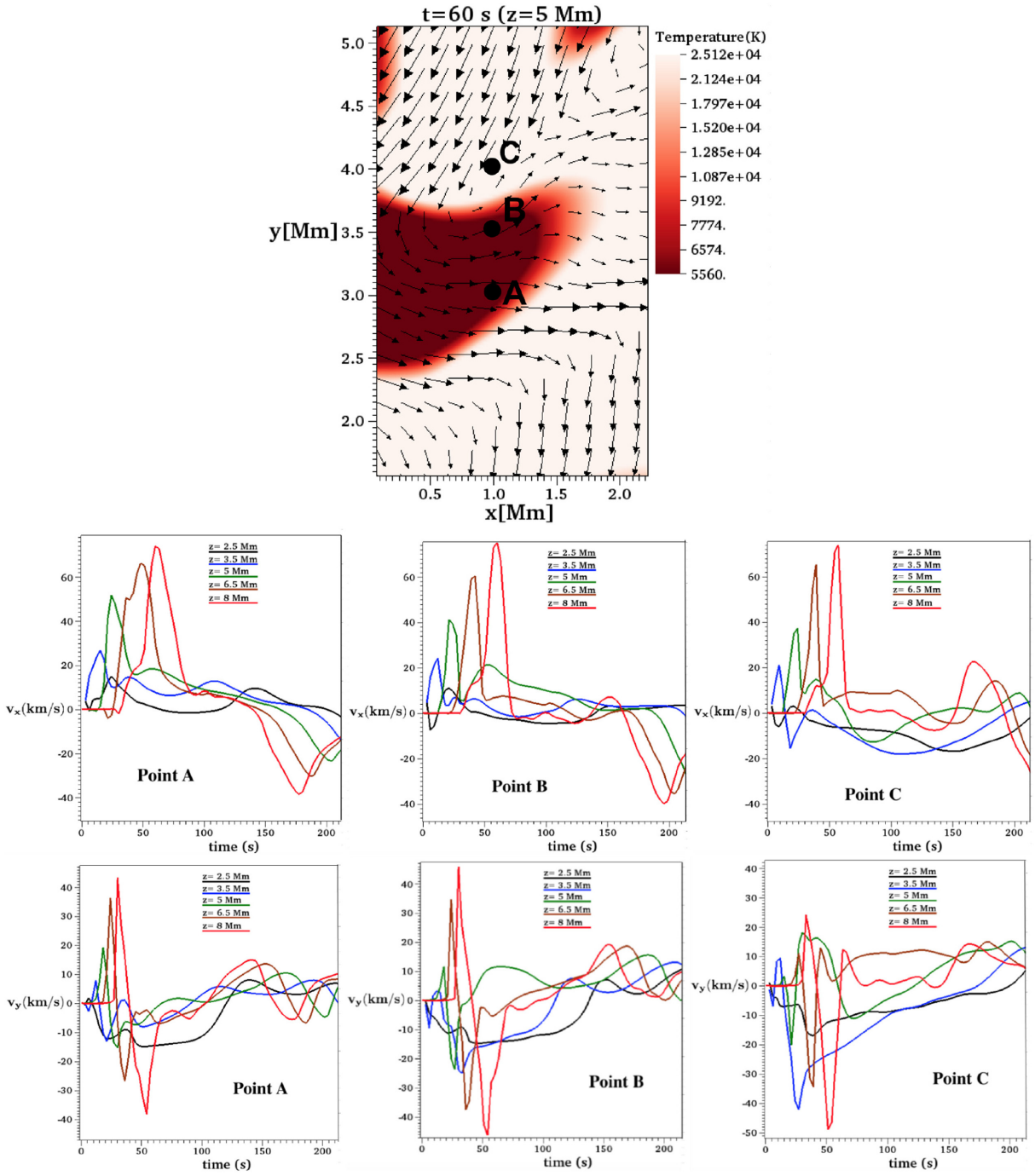

Figure 2. In the top we show the region where v_x and v_y are measured. The colour labels the temperature in the plane $z = 5$ Mm at time $t = 60$ s, where the structure of spicule and the circulation of the vector velocity field is clearly seen. In the middle and bottom panels, we show the time series of v_x and v_y in km s^{-1} of the volume elements at the points A, B, and C measured at various planes of constant height.

adaptive choice of flux formula between HLLC and HLLE, combined with MINMOD and MC limiters.

For the initial magnetic field, we use a 3D potential (current-free) configuration extrapolated from a simulated quiet-Sun photospheric field, obtained from a large-scale, high-resolution, self-consistent simulation of solar magnetoconvection in a bipolar photospheric region with the MURAM code (Vögler et al. 2005; Shelyag, Mathioudakis & Keenan 2012). The computational box has a size of 480 × 480 × 400 pixels, with a spatial resolution of 25 km in all directions. The magnetic field lines of the 3D configuration are shown in the left-hand side of Fig. 1, and it is in this domain where the cross-cuts and further analysis are performed.

In order to model the atmosphere we choose the numerical domain to cover part of the interconnected solar photosphere, chromosphere, and corona (see Fig. 1). For this the atmosphere is initially assumed to be in hydrostatic equilibrium. The temperature field is considered to obey the semi-empirical C7 model of the chromosphere transition region (Avrett & Loeser 2008) and is

Downloaded from https://academic.oup.com/mnras/article-abstract/484/2/1936/5287990 by University of Northumbria user on 04 April 2019

distributed consistently with observed line intensities and profiles from the SUMER atlas of the extreme ultraviolet spectrum (Curdt et al. 1999). The photosphere is extended to the solar corona as described by Fontela, Avrett & Loeser (1990) and Griffiths et al. (1999). The temperature $T(z)$ and mass density $\rho(z)$ are functions of height z and are shown in Fig. 1, where the transition region shows its characteristic steep gradient.

Once the magnetic field and atmosphere model are set in the computational domain ($240 \times 240 \times 400$ grid cells with a resolution of 25 km in each direction), the plasma evolves due to the inclusion of resistivity according to the EGLM equations. For our analysis, we focus on a 3D numerical box with unigrid discretization of size $x \in [0, 6]$, $y \in [0, 6]$, $z \in [0, 10]$ Mm. In Section 3, we analyse the transverse and rotational motions in the jet and their observational signatures.

3 PLASMA MOTIONS IN THE JET

3.1 Transverse motions

A property to look into is the transverse displacement of the jet and investigate if it is actually oscillating in a kink-like manner. We measure the velocity components v_x and v_y in time at three different points near and within the spicule, points A ($x = 1$, $y = 3$, z) Mm, points B ($x = 1$, $y = 3.5$, z) Mm, and points C ($x = 1$, $y = 4$, z) Mm, for various values of z. Near these points the vector velocity field rotates as is illustrated at the top of Fig. 2. We measure the value of the velocity components at heights $z = 2.5$, 3.5, 5, 6.5, and 8 Mm. The results displayed in Fig. 2 tell us about the motion along the x and y directions. For example, the horizontal component of velocity v_x at the various heights in point A shows transverse displacements with high amplitudes at the top of jet and small at the bottom. We can also see a change of sign, which indicates a transverse oscillation of at least one period. The behaviour of v_x at points B and C is similar to that at point A. In the case of the v_y component at point A, we can see strong motions at the top, in particular there is a clear change of sing between 0 and 100 s, then we can identify oscillatory behaviour at all heights, which is also clear at points B and C. By comparing the behaviour of v_x and v_y, we can conclude that the jet shows rotational motion, i.e. velocity components are out of phase, which will be reinforced by the following analysis.

Aside from analysing the transverse motion at individual points in space, we can also identify the bulk transverse displacement of the jet in a horizontal cross-cut across the jet shown in a logarithm of temperature on the left-hand side of Fig. 3. We measure this bulk transverse motion at a height of 7 Mm along a horizontal slice of length 3 Mm (blue line) centred at the mid-point of the domain in the y-direction (black line) as shown on the left-hand side of Fig. 3. A time-distance plot of the logarithm of temperature along this slice as a function of time is shown on the right-hand side of Fig. 3. From the time-distance plot, we can see that from time $t =$ 50 s the jet starts moving to the left-hand side until about time $t =$ 150 s, jet starts moving to the right until it is displaced a horizontal distance of 3 Mm. This shows that simulated jet actually has a significant transverse motion during its lifetime. This phenomenon is also observed widely in spicule observations, see e.g. De Pontieu et al. (2007b). To estimate the average speed of the transverse displacements, we indicate the centre of the jet at the times of maximum and minimum displacement up to 150 s with horizontal dashed blue lines on the right-hand side of Fig. 3. The distance between the two lines is about 0.7 Mm (700 km) and the time between them is about 100 s, therefore the average speed is about 7 km s^{-1}.

3.2 Rotational motions

Another important property of type II spicules to look at is whether they are twisted, rotated, or show an azimuthal flow component. Doppler shift observations of various emission lines in the limb suggest that type II spicules are rotating (De Pontieu et al. 2012; Sekse et al. 2013; Sharma et al. 2017). From our simulation it is possible to study the behaviour of the velocity components v_x and v_z inside the jet in order to track possible rotational or twisting motions. A similar analysis was carried out by Pariat et al. (2016) to identify torsional/twisting motions of coronal jets. In our case we show temperature contours with constant value of 10^4 K coloured with the distribution of v_x at times $t = 30$, 45, 60, 90, 105, 120, 150, 180, and 210 s in Fig. 4.

For the perspective used in this case, the blue colour represents motion towards the reader and red colour represents motion away from the observer. For instance, at time $t = 30$ s the jet starts to develop and shows both red- and blue-shifted plasma. By times $t =$ 45 and 60 s, the motions are predominantly towards the observer with counter-motion developing at the top of the jet. At time $t = 90$ s,

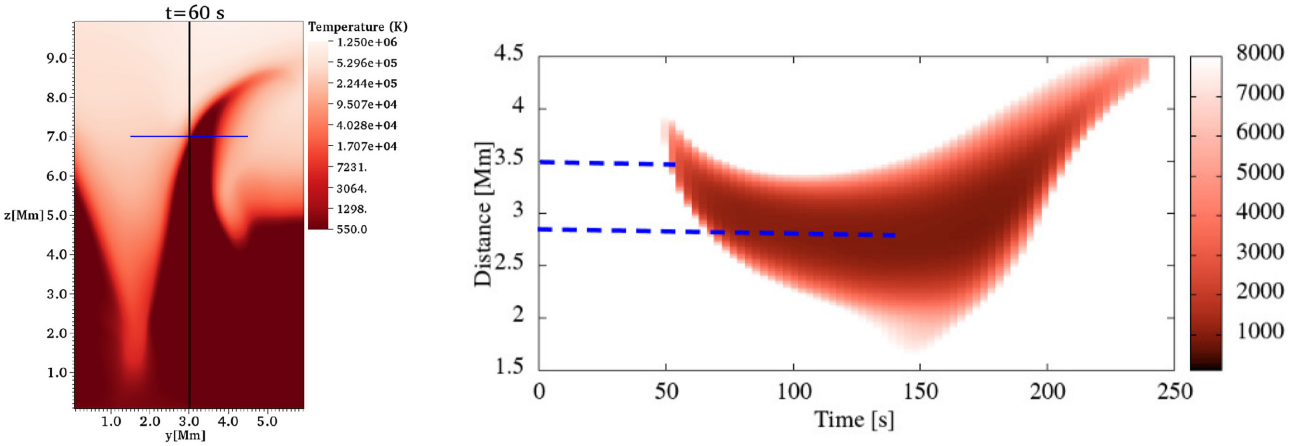

Figure 3. (Left) Snapshot of the logarithm of temperature (K) at time $t = 60$ s, vertical line in black at $y = 3$ Mm and horizontal line in blue from $y = 1.5$ Mm to $y = 4.5$ Mm at $z = 7$ Mm. (Right) The time-distance plot of logarithm of temperature (K) and dashed lines to estimate the average transverse speed.

Downloaded from https://academic.oup.com/mnras/article-abstract/484/2/1936/5287990 by University of Northumbria user on 04 April 2019

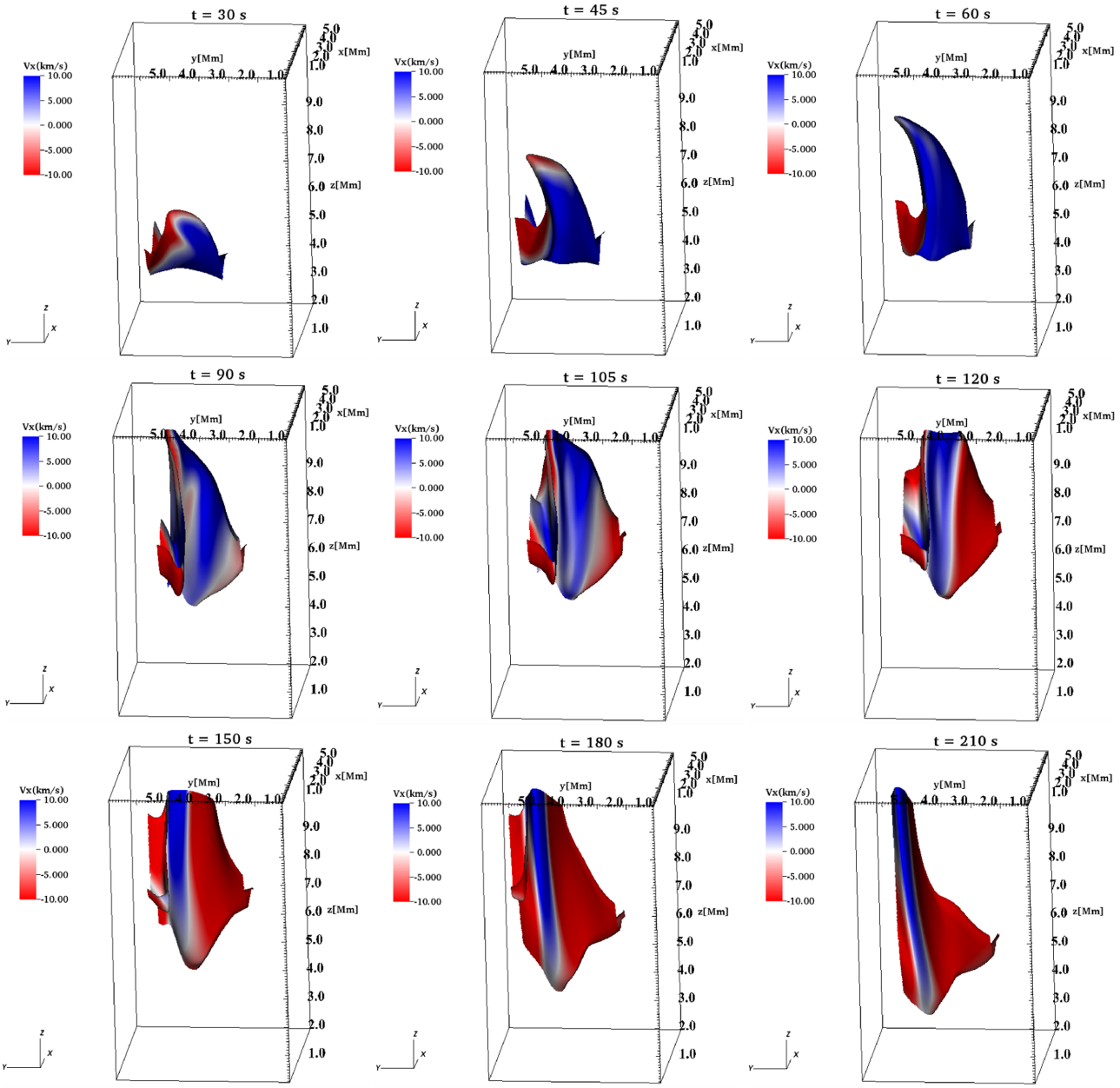

Figure 4. Snapshots of a temperature contour at various times. The jet is represented by an isosurface of the plasma temperature equal to 10^4 K. The colour code labels the value of v_x. In this perspective blue indicates motion towards the reader and red towards inside the page.

the predominant motion towards the observer and some counter-motion still persists at the top of the jet. This dual behaviour lasts through times $t = 105$ and $t = 120$ s. At times $t = 150$, 180, and 210 s the jet shows a velocity structure represented by a red–blue asymmetry across its width. The time evolution of the jet from the simulation (Fig. 4) also shows strong resemblance to the observations of a spicule seen off-limb in Hα (Fig. 5). The imaging-spectroscopy data used in the study were taken from the CRisp Imaging SpectroPolarimeter (CRISP) at the Swedish Solar Telescope (SST) on 2014 June 05, during 11:53–12:34 ut, centred at $x_c = 876$ arcsec, $y_c = 343$ arcsec. The data were processed using the Multi-Object Multi Frame Blind Deconvolution [MOMFBD; Van Noort, Der Voort & Löfdahl (2005)] image restoration technique. The off-limb region was scanned at ±4 positions w.r.t. the line core (6563 Å) on the line profile, with final science data had a pixel size of 0″.059 (∼43 km), angular resolution of 0″.13 (∼ 86 km), and a cadence of 5 s. The data set was also used previously by Shetye et al. (2016) to compare the image restoration techniques for chromospheric features. The unsharp mask intensity image (Fig. 5a) of this spicule suggests it is launched from an inverted Y-shaped structure (Shibata et al. 2007; He et al. 2009), associated with reconnection. The estimated Doppler shift profile (V_x) at discrete time-steps of the spicule evolution shows striking similarities with the simulated jet. Fig. 5(b) showcases the early rise-phase of the spicule ($t = 10$ s) as it starts to penetrate through the ambient chromospheric environment, as seen in Fig. 4 ($t = 30$ s). At the middle-phase of its evolution (Fig. 4; $t = 105$ s), the spicule attains a mainly blue-shift Doppler profile, indicating bulk motion towards the observer as shown in Fig. 5(c). However, at the late-phase of the spicule's ascent, the apex has developed an asymmetric red-blue

Downloaded from https://academic.oup.com/mnras/article-abstract/484/2/1936/5287990 by University of Northumbria user on 04 April 2019

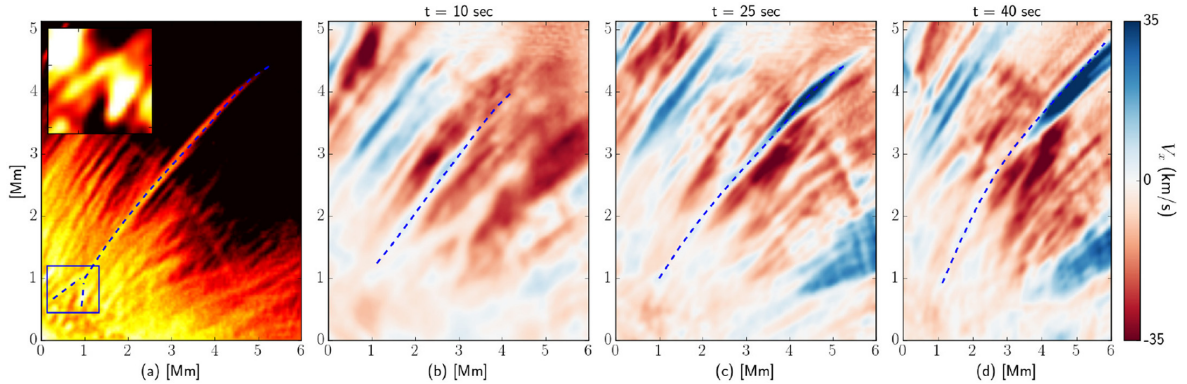

Figure 5. Left to right: Panels show a spicule (traced as dashed-line) off-limb, observed in Hα wavelength (a), with temporal evolution of the LOS Doppler velocity estimates (b–d). The unsharp-masked intensity image (a) shows inverted Y-shaped structure (zoomed in inset) at the spicule footpoint (highlighted in box) suggestive of a magnetic reconnection process. Doppler estimates reveal the longitudinal rise of the spicule with its dominant motion towards the observer (b–c). The development of rotational motion is indicated by the enhanced red–blue asymmetric profile at the apex of spicule (d).

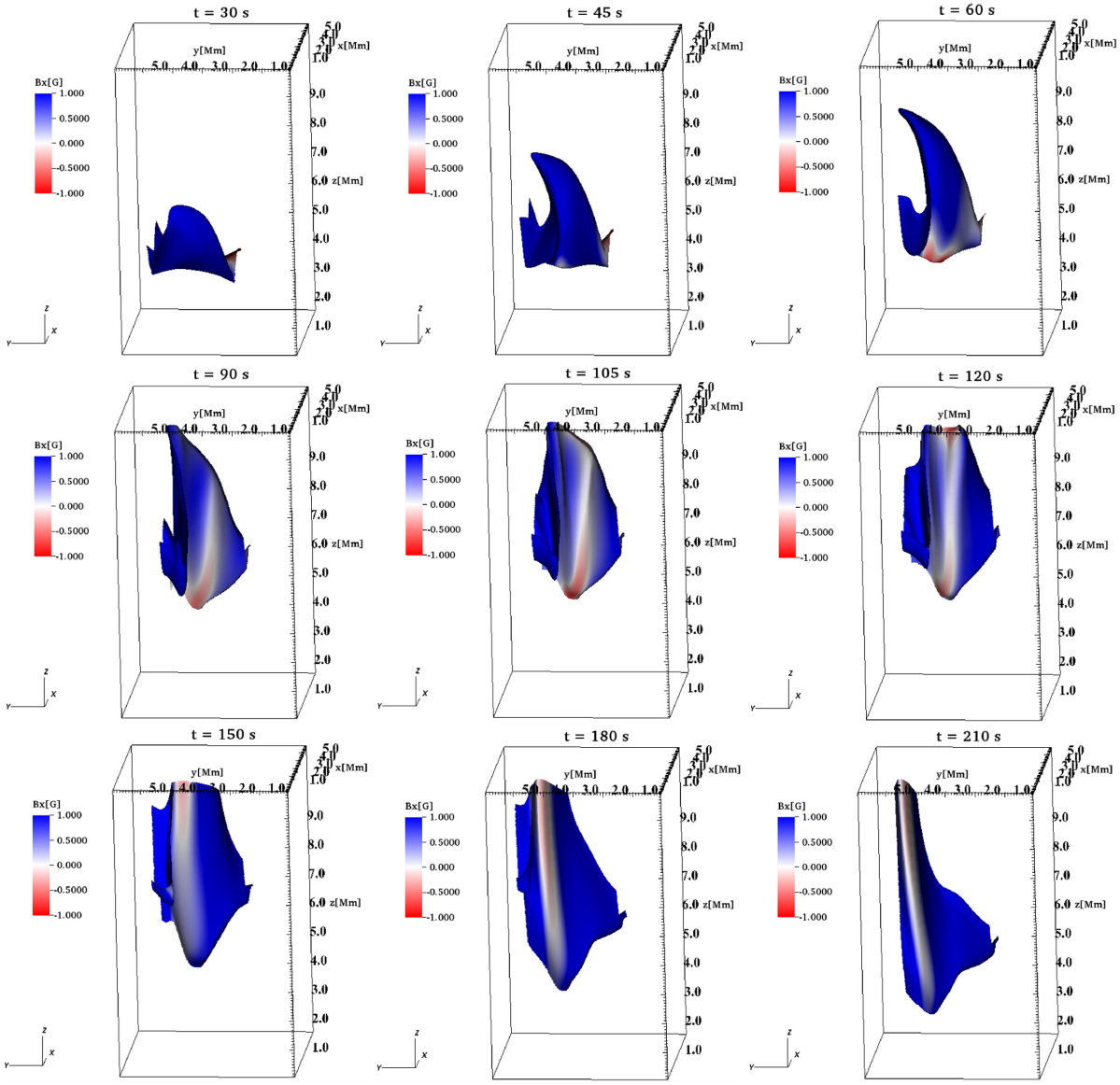

Figure 6. Snapshots of a temperature contour at various times. The jet is represented by an isosurface of the plasma temperature equal to 10^4 K. The colour code labels the value of B_x.

Downloaded from https://academic.oup.com/mnras/article-abstract/484/2/1936/5287990 by University of Northumbria user on 04 April 2019

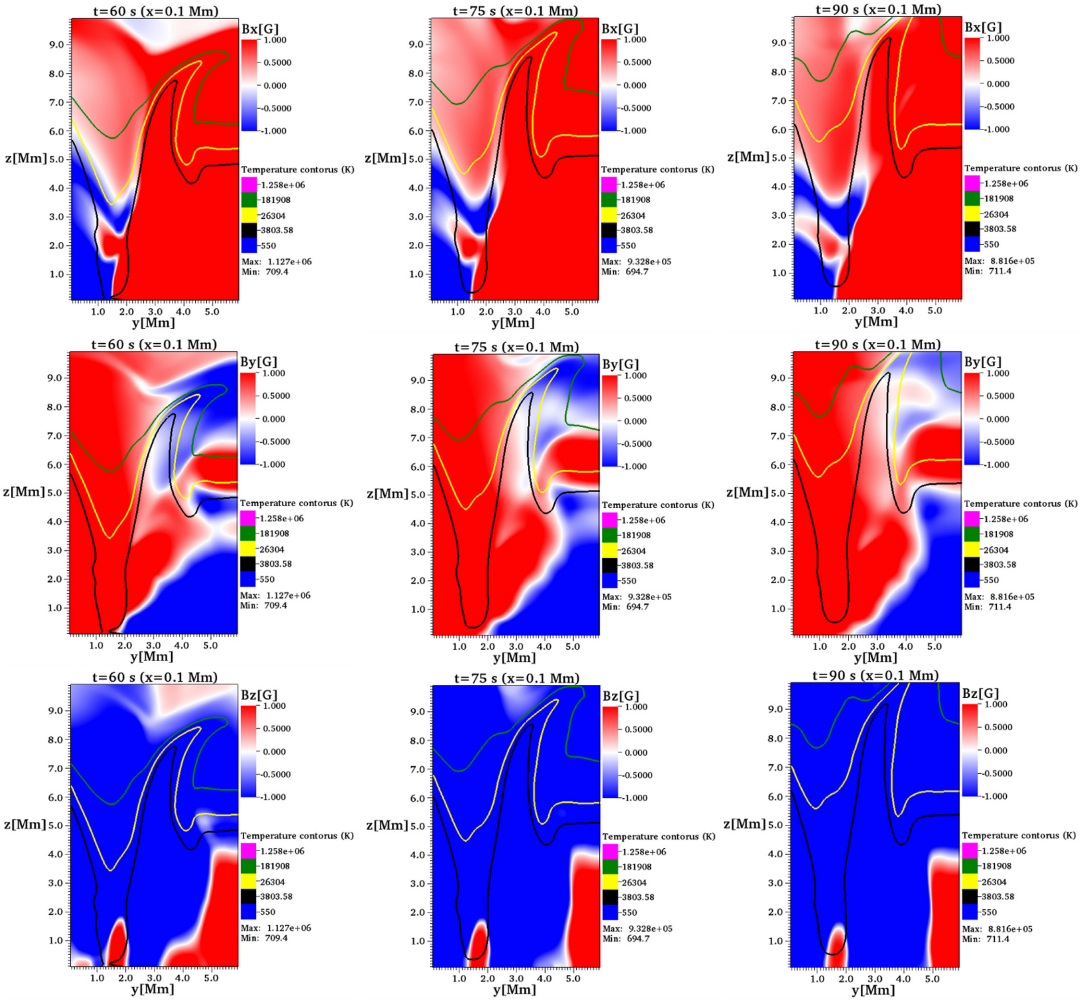

Figure 7. Snapshots of the magnetic field components B_x, B_y, B_z (G) and temperature contours (K) in a cross-cut at $x = 0.1$ Mm at times 60, 75, and 90 s.

Doppler profile (Fig. 5d), indicating rotational motion, similar to the simulated jet (Fig. 4, $t = 180$ s). The rotational motion is prevalent at height above 3 Mm, as is also seen in the simulation.

Also, the diagnostics shown in the time series of the velocity components at points A, B, and C in Fig. 2 together with Fig. 4 indicate rotational motions of the jet.

Apart from the comparison of the red-blue shift with the observations, we can also link the x component of the magnetic field B_x from our simulation to the LOS measurements of the magnetic fields in spicules (López Ariste & Casini 2005; Centeno, Trujillo Bueno & Asensio Ramos 2010; Orozco Suárez, Asensio Ramos & Trujillo Bueno 2015); therefore, in Fig. 6 we show temperature contours with constant value of 10^4 K coloured with the distribution of B_x at different times. For instance, at time $t = 30$ s the jet shows mainly positive values of the magnetic field, a behaviour that lasts until $t = 60$ s. At time $t = 90$ s, we can see the appearance of negative values from the bottom of the jet, which last until $t = 120$ s. At the three last times $t = 150$, 180, and 210 s the negative values appear from the top of the jet. In addition, in Fig. 7 we show the magnetic field components B_x, B_y, B_z and temperature contours in a cross-cut at $x = 0.1$ Mm for three different times, this figure is similar to figs 5–7 of paper by González-Avilés et al. (2018). For instance at the top of Fig. 7, we can see positive values of B_x along the jet and the predominance of negative values at the bottom of the jet for the three times. At the middle, we can see negative values of B_y at the top of the jet, while there is a predominance of positive values of B_y at the bottom for the three times. At the bottom, we see that the B_z component is predominantly negative along the jet for three times.

3.3 Vertical motions

In Fig. 8, we show the isosurface of temperature coloured with the values of v_z, which helps to track the vertical motion of the jet, for instance at times $t = 30$, 45, and 60 s, the jet practically shows upward motion from the middle to the top. By times $t = 90$, 105, and 120 s, the amplitude of vertical motion starts to decrease at the bottom of the jet. Finally, at times $t = 150$, 180, and 210 s the jet starts moving downwards, in particular this behaviour is consistent with the observed vertical motion with velocities of the order 110 km s^{-1} in type II spicules (Skogsrud, Roupe van Der Voort & De Pontieu 2014).

4 CONCLUSIONS

In this paper by analysing temperature isosurfaces to localize the jet, together with the analysis of the horizontal velocity components, we find that the development of a red–blue asymmetry across the jet is due to rotational motion. Interestingly, the rotational motion

Downloaded from https://academic.oup.com/mnras/article-abstract/484/2/1936/5287990 by University of Northumbria user on 04 April 2019

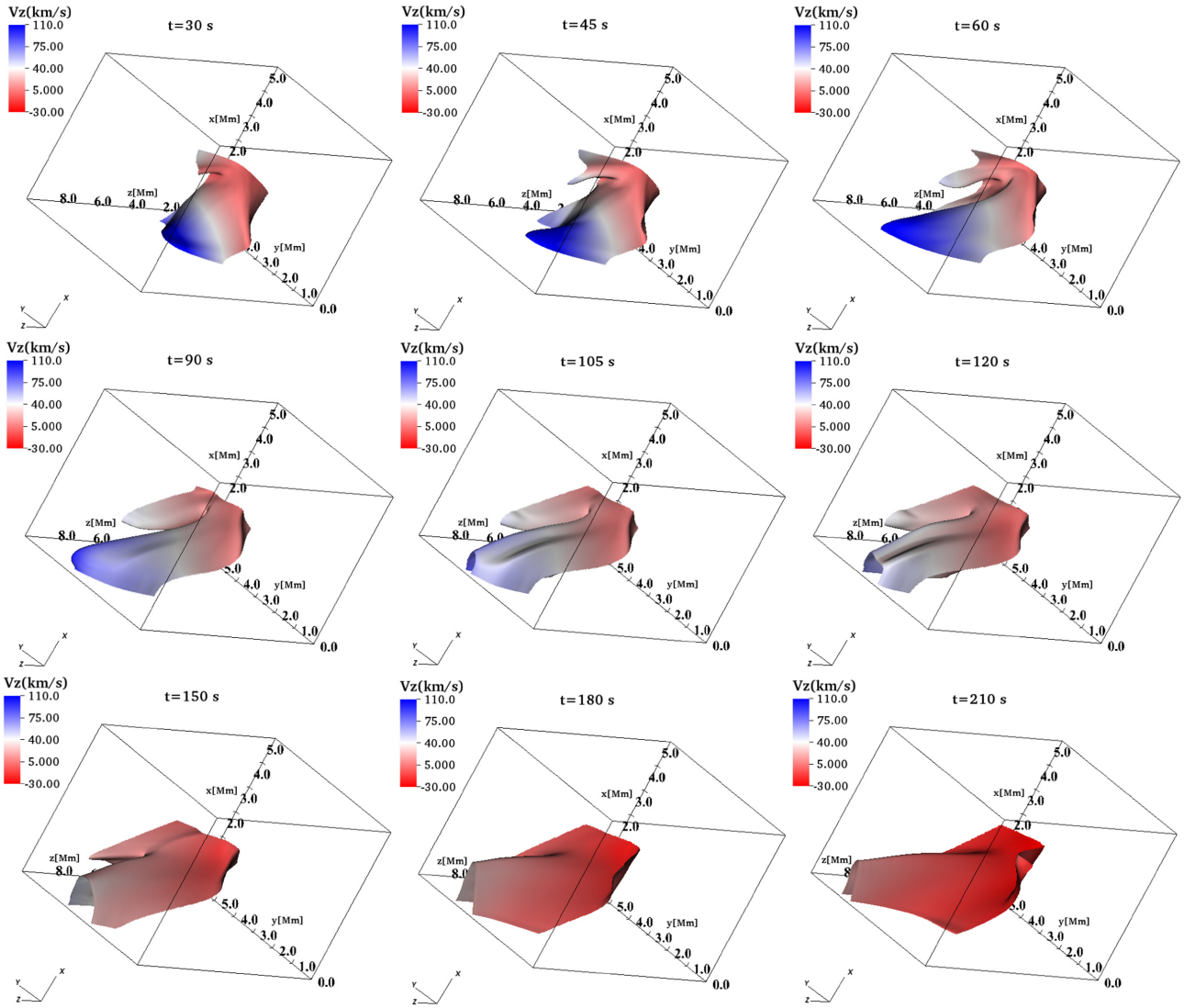

Figure 8. Snapshots of a temperature contour at various times. The jet is represented by an isosurface of the plasma temperature equal to 10^4 K. The colour code labels the value of v_z. The colour red and blue indicates downward and upward velocity, respectively.

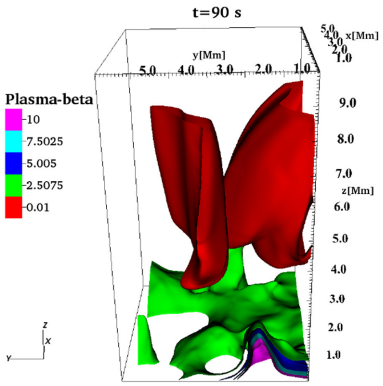

Figure 9. Contours of plasma β at time $t = 90$ s. The contours indicate that magnetic field is dominant in the region where the spicule is formed as is shown in Fig. 4.

is initially clockwise and then begins to move in an anti-clockwise direction, indicating the presence of torsional motion. By analysing the time series of v_x and v_y at points near and within the jet at different heights we showed that the rotational motion is generated in its upper region. In addition, by calculating a time-distance plot of the logarithm of temperature in a horizontal cross-cut at a height of 7 Mm it was shown that the jet also undergoes a considerable transverse displacement.

Additionally, we have presented observational support of rotational motion in an off-limb spicule appearing in the corona (and not being generated from below) in Fig. 5(d). We can also see the simulated jet has a dual behaviour (i) transverse motion at the foot (0–3 Mm) and (ii) twisted motion at the middle and top parts (3–10 Mm). The rotational type motion (initially clockwise and after anti-clockwise) can be interpreted as torsional starting at the top of the jet, when it reaches a region where the magnetic field dominates $\beta < 1$ as shown in Fig. 9 and the Lorentz force is also bigger than pressure gradients $|\mathbf{J} \times \mathbf{B}| > |\nabla p|$ as shown in fig. 7 of paper by González-Avilés et al. (2018). This is important as it shows that torsional waves can be generated directly in the corona and therefore

Downloaded from https://academic.oup.com/mnras/article-abstract/484/2/1936/5287990 by University of Northumbria user on 04 April 2019

the whole wave energy (i.e without any loses due to propagation from the photosphere and dynamic chromosphere to the corona, as is usually suggested) can be dissipated in the corona. For example, regions with ($\beta < 1$) are perfect for the decay of torsional Alfvén waves into kinetic Alfvén waves, see e.g. cross-scale nonlinear coupling and plasma energization by Alfvén waves (Voitenko & Goossens 2005), excitation of kinetic Alfvén turbulence by MHD waves and energization of space plasmas (Voitenko & Goossens 2004) or the transformation of MHD Alfvén waves in space plasma (Fedun, Yukhimuk & Voitsekhovskaya 2004).

From a nearly vertical perspective of the jet, the vertical component of the velocity shows a blue–red shift that is similar to the one observed in the transition region and coronal lines as shown in fig. 18 of Martínez-Sykora et al. (2013), where the Doppler shifts correspond to velocities within the range -8 to 8 km s^{-1}. Finally, although there is no magnetoconvection, in the simulated plasma jet we conclude that rotational motion can still occur naturally at coronal heights without the need of any photospheric driver, e.g. granular buffeting or vortex motion. In fact, we have shown that such jets could be an *in situ* driver of torsional Alfvén waves in the corona.

ACKNOWLEDGEMENTS

This research is partly supported by the following grants: Royal Society-Newton Mobility Grant NI160149, CIC-UMSNH 4.9, and CONACyT 258726 (Fondo Sectorial de Investigación para la Educación). The simulations were carried out in the Big Mamma cluster at the LIASC-IFM. VF and GV thank the STFC for their financial support. JG gratefully acknowledges DGAPA postdoctoral grant to Universidad Nacional Autónoma de México (UNAM). RS acknowledges support by the Spanish Ministry of Economy and Competitiveness (MINECO) through project AYA2016-80881-P. Visualization and analysis of the simulations data were done with the use of the VISIT software package. The authors thank to G. Doyle and E. Scullion for providing the observational data that were collected using the Swedish 1-m Solar Telescope. This telescope is operated on the island of La Palma by the Institute for Solar Physics of Stockholm University in the Spanish Observatorio del Roque de los Muchachos of the Instituto de Astrofísica de Canarias. The Institute for Solar Physics is supported by a grant for research infrastructures of national importance from the Swedish Research Council (registration number 2017-00625). The authors also wish to acknowledge the DJEI/DES/SFI/HEA Irish Centre for High-End Computing (ICHEC) for the provision of computing facilities and support. This work also greatly benefited from the discussions at the ISSI workshop 'Towards Dynamic Solar Atmospheric Magneto Seismology with New Generation Instrumentation'.

REFERENCES

Avrett E. H., Loeser R., 2008, ApJS, 175, 229
Beckers J. M., 1968, Sol. Phys., 3, 367
Beckers J. M., 1972, ARA&A, 10, 73
Centeno R., Trujillo Bueno J., Asensio Ramos A., 2010, ApJ, 708, 1579
Cheung M. C. M. et al., 2015, ApJ, 801, 83
Curdt W., Tian H., 2011, A&A, 532, L9
Curdt W., Heinzel P., Schmidt W., Tarbell T., Uexkull V., Wilken V., 1999, in Wilson A., ed., ESA SP-448, in Magnetic Fields and Solar Processes, Proc. 9th European Meeting on Solar Physics. ESA, Noordwijk, p. 177
Curdt W., Tian H., Kamio S., 2012, Sol. Phys., 280, 417
De Pontieu B., Erdélyi R., James S. P., 2004, Nature, 430, 536
De Pontieu B., McIntosh S., Hansteen V. H., 2007a, PASJ, 59, 655
De Pontieu B. et al., 2007b, Science, 318, 1574
De Pontieu B., McIntosh S. W., Hansteen V. H., Schrijver C. J., 2009, ApJ, 701, L1
De Pontieu B. et al., 2011, Science, 331, 55
De Pontieu B., Carlsson M., Rouppe van der Voort L. H. M., Rutten R. J., Hansteen V. H., Watanabe H., 2012, ApJ, 752, L12
Dere K. P., Bartoe J.-D. F., Brueckner G. E., 1989, Sol. Phys., 123, 41
Fedun V. N., Yukhimuk A. K., Voitsekhovskaya A. D., 2004, J. Plasma Phys., 70, 06
Fontela J. M., Avrett E. H., Loeser R., 1990, ApJ, 355, 700
González-Avilés J. J., Guzmán F. S., Fedun V., Verth G., Shelyag S., Regnier S., 2018, ApJ, 856, 176
Griffiths N. W., Fisher G. H., Woods D. T., Siegmund H. W., 1999, ApJ, 512, 992
Hansteen V. H., De Pontieu B., Ruoppe van der Voort L., van Noort M., Carlsson M., 2006, ApJ, 647, L73
He J., Marsch E., Tu C., Tian H., 2009, ApJ, 705, L217
Jiang R. L., Fang C., Chen P. F., 2012, Comp. Phys. Comm., 183, 1617
Kayshap P., Murawski K., Srivastava A. K., Dwivedi B. N., 2018, A&A, 616, A99
Kuridze D., Morton R. J., Erdélyi R., Dorrian G. D., Mathioudakis M., Jess D. B., Keenan F. P., 2012, ApJ, 750, 51
Liu W., Berger T. E., Title A. M., Tarbell T. D., 2009, ApJ, 707, L37
Liu W., Berger T. E., Title A. M., Tarbell T. D., Low B. C., 2011, ApJ, 728, 103
López Ariste A., Casini R., 2005, A&A, 436, 325
Martínez-Sykora J., Hansteen V., Carlsson M., 2009, ApJ, 702, 129
Martínez-Sykora J. et al., 2013, ApJ, 771, 66
Martínez-Sykora J., De Pontieu B., Hansteen V. H., Roupe van der Voort L., Carlsson M., Pereira T. M. D., 2017, Science, 356, 1269
Matsumoto T., Shibata K., 2010, ApJ, 710, 1857
McIntosh S. W., de Pontieu B., Carlsson M., Hansteen V., Boerner P., Goossens M., 2011, Nature, 475, 477
McLaughlin J. A., Verth G., Fedun V., Erdélyi R., 2012, ApJ, 749, 30
Nishizuka N. et al., 2008, ApJ, 683, L83
Okamoto T. J., De Pontieu B., 2011, ApJ, 736, L24
Orozco Suárez D., Asensio Ramos A., Trujillo Bueno J., 2015, ApJ, 803, L18
Pariat E., Dalmasse K., DeVore C. R., Antiochos S. K., Karpen J. T., 2016, A&A, 596, A36
Pereira T. M. D., De Pontieu B., Carlsson M., 2012, ApJ, 759, 18
Pike C. D., Mason H. E., 1998, Sol. Phys., 182, 333
Scullion E., Erdélyi R., Fedun V., Doyle J. G., 2011, ApJ, 743, 14
Secchi A., 1878, Die Sterne: Grundzuge der Astronomie der Fixsterne. Brockhaus, Germany
Sekse D. H., Rouppe van der Voort L., De Pontieu B., 2012, ApJ, 752, 108
Sekse D. H., Rouppe van der Voort L., De Pontieu B., Scullion E., 2013, ApJ, 769, 44
Sharma R., Verth G., Erdélyi R., 2017, ApJ, 840, 96
Shelyag S., Mathioudakis M., Keenan F. P., 2012, ApJ, 753, L22
Shetye J., Doyle J. G., Scullion E., Nelson C. J., Kuridze D., Henriques V., Woeger F., Ray T., 2016, A&A, 589, A3
Shibata K., Nishikawa T., Kitai R., Suematsu Y., 1982, Sol. Phys., 77, 121
Shibata K. et al., 2007, Science, 318, 5856
Skogsrud H., Roupe van Der Voort L., De Pontieu B., 2014, ApJ, 795, L23
Sterling A. C., 2000, Sol. Phys., 196, 79
Sterling A. C., Harra L. K., Moore R., 2010a, ApJ, 722, 1644
Sterling A. C., Moore R., DeForest C. E., 2010b, ApJ, 714, L1
Suematsu Y., Wangm H., Zirin H., 1995, ApJ, 450, 411
Suematsu Y., Ichimoto K., Katsukawa Y., Shimizu T., Okamoto T., Tsuneta S., Tarbell T., Shine R. A., 2008, in Matthews S. A., Davis J. M., Harra L. K., eds, ASP Conf. Ser. Vol. 397, First Results from Hinode. Astron. Soc. Pac., San Francisco, p. 27
Tavabi E., Koutchmy S., Golub L., 2015, Sol. Phys., 290, 2871
Tian H. et al., 2014, Science, 346, 1255711

Downloaded from https://academic.oup.com/mnras/article-abstract/484/2/1936/5287990 by University of Northumbria user on 04 April 2019

Tomczyk S., McIntosh S. W., Keil S. L., Judge P. G., Schad T., Seeley D. H., Edmondson J., 2007, Science, 317, 1192
Van Noort M., Der Voort L. R. V., Löfdahl M. G., 2005, Sol. Phys., 228, 191
Vögler A., Shelyag S., Schüssler M., Cattaneo F., Emonet T., Linde T., 2005, A&A, 429, 335
Voitenko Y., Goossens M., 2004, Nonlin. Processes Geophys., 11, 535
Voitenko Y., Goossens M., 2005, Phys. Rev. Lett., 94, 135003
Zaqarashvili T. V., Erdélyi R., 2009, Space Sci. Rev., 149, 355

This paper has been typeset from a TEX/LATEX file prepared by the author.

Downloaded from https://academic.oup.com/mnras/article-abstract/484/2/1936/5287990 by University of Northumbria user on 04 April 2019